ACS APPLIED ELECTRONIC MATERIALS

pubs.acs.org/acsaelm Article

# Development of Inks with Fillers of $NbS_3$ Quasi-One-Dimensional Charge-Density-Wave Material

Tekwam Geremew, Maedeh Taheri, Nicholas Sesing, Subhajit Ghosh, Fariborz Kargar,* Tina T. Salguero, and Alexander A. Balandin*

Cite This: *ACS Appl. Electron. Mater.* 2024, 6, 4653−4660 Read Online

ACCESS | Metrics & More | Article Recommendations

**ABSTRACT:** We report on the solution processing and testing of electronic ink composed of quasi-one-dimensional $NbS_3$ charge-density-wave fillers. The ink was prepared by liquid-phase exfoliation of $NbS_3$ crystals into high-aspect-ratio quasi-1D fillers dispersed in a mixture of isopropyl alcohol and ethylene glycol solution. The results of the electrical measurements of two-terminal electronic test structures printed on silicon substrates reveal resistance anomalies in the temperature range of ∼330−370 K. It was found that the changes in the temperature-dependent resistive characteristics of the test structures originate from the charge-density-wave phase transition of individual $NbS_3$ fillers. The latter confirms that the exfoliated $NbS_3$ fillers preserve their intrinsic charge-density-wave condensate states and can undergo phase transitions above room temperature even after chemical exfoliation processes and printing. These results are important for developing "quantum inks" with charge-density-wave fillers for the increased functionality of future solution-processed electronics.

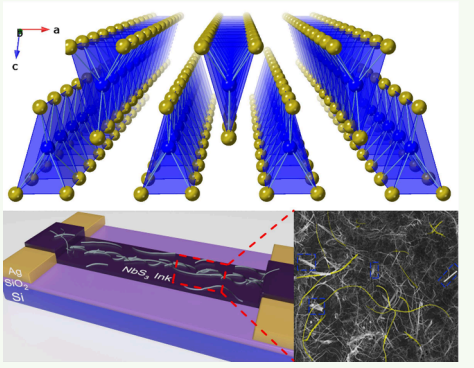


**KEYWORDS:** *one-dimensional materials, charge density waves, printed electronics, solution-processed electronics, quantum materials, $NbS_3$*



## 1. INTRODUCTION

Printed electronics with inks of solution-processed low-dimensional materials, such as graphene and transition metal dichalcogenides (TMDs), have attracted significant interest owing to the potential for offering versatile device applications at lower manufacturing costs.[1−4] Printing adopts an additive manufacturing technique to deposit micro- and nanoscale materials on substrates with different rigidity through various printing technologies.[5−8] Among the printing approaches, inkjet printing is considered one of the promising technologies owing to its mask-free printing requirements, large scale, and high manufacturing throughput.[9−13] Generally, in inkjet printing, solution-based inks with fillers of electrically conductive, insulative, or semiconductive nature are deposited onto flexible polymer or conventional silicon substrates.[14−17] For example, graphene-based conductive inks, printed on flexible substrates, have given rise to device applications such as humidity sensors, electrochemical sensors, transistors, photovoltaic cells, and wireless data communications.[18−21] Other two-dimensional (2D) TMDs, such as $MoS_2$ and $WS_2$ ink devices, have been widely employed for printed optoelectronics devices, sensor applications, logic gates, and energy storage devices.[22−24]

Although printing with 2D and other low-dimensional semiconductor inks offers exciting opportunities for novel electronics, it suffers from a fundamental shortcoming. That is the overall electric transport in any printed channel with semiconducting fillers will be dominated by the electron hopping mechanism.[25−27] In a printed device with semiconducting fillers, the electric conductivity in individual fillers is governed by band-type charge transport. However, at the filler−filler interfaces, charge hopping will become the dominant transport mechanism under any conditions. This situation explains why printed devices with semiconducting fillers demonstrate much lower mobilities compared to devices fabricated with conventional cleanroom techniques.[28,29] Furthermore, other undesired effects, such as defects and impurities, are usually induced in the fillers during the ink preparation and make the situation even worse. As a result, it is challenging to maintain the original properties of pure crystalline semiconductor materials in their disordered form within the ink. To take advantage of opportunities offered by printing and to overcome the challenges described above, one can think of utilizing functional low-dimensional materials with

**Received:** April 12, 2024
**Revised:** May 14, 2024
**Accepted:** May 23, 2024
**Published:** June 4, 2024

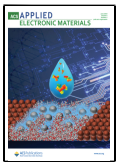




https://doi.org/10.1021/acsaelm.4c00646
*ACS Appl. Electron. Mater.* 2024, 6, 4653−4660

unique properties, such as charge-density-wave (CDW) materials.

The CDW phenomena are the condensate phase effects, observed in some quasi-one-dimensional (1D) and quasi-2D materials.[30−33] It manifests as a periodic modulation of electron charge density coupled with a corresponding periodic distortion of the underlying crystal lattice.[33] This effect results in anomalies in temperature-dependent charge transport characteristics that can be harnessed for electronic devices, such as voltage-controlled oscillators.[34,35] To design CDW-based printed devices, the first challenge to be addressed is whether such materials can preserve their CDW condensate properties after the chemical processes required for ink preparation.

Here, we report on the preparation of functional inks with one-dimensional (1D) $NbS_3$ CDW material as a filler. $NbS_3$ belongs to the family of transition metal trichalcogenides (TMTs), a class of 1D van der Waals (vdW) compounds where M is a transition metal and X is a chalcogen atom.[36] Among the $MX_3$ materials, $NbS_3$ has attracted much attention owing to its polymorphism and the presence of the CDW phases above room temperature (RT).[37−39] Similar to other $MX_3$ materials, $NbS_3$ has a chain-like structure with strong covalent bonds in the chain direction. Chains are arranged as bilayers through Nb−S interactions, and these layers are held together by relatively weak vdW forces that allow top-down nanostructuring via mechanical or liquid-phase exfoliation (LPE) techniques.[37,40] This is a key feature because the resulting quasi-1D $NbS_3$ nanowires have high aspect ratios and mechanical flexibility—properties that allow electrical percolation to be reached at lower concentrations.[15,41] This characteristic is crucial for the preparation of inks with desired thermophysical properties and for achieving a reasonable electrical conductivity after the printing of a few layers.

## 2. MATERIAL CHARACTERIZATIONS

The various $NbS_3$ polymorphs differ in Nb−Nb bonding along the chains as well as in the specific packing arrangements of chains and bilayers. Figure 1a shows the basic chain and bilayer

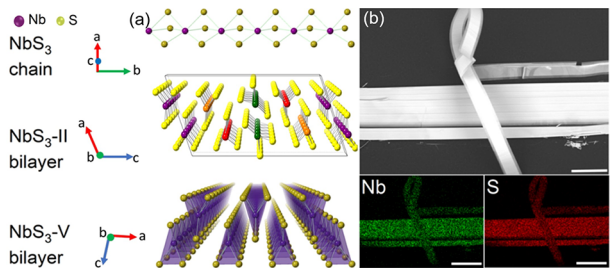


**Figure 1.** (a) Crystal structures of the $NbS_3$ single chain and bilayer structures of $NbS_3$-II and $NbS_3$-V polymorphs. (b) Representative SEM imaging and EDS elemental mapping of the as-grown $NbS_3$ crystals. The scale bar is 50 $\mu$m.

structures of $NbS_3$-II and $NbS_3$-V, both of which are metallic.[39,42] The polymorphs belong to the $P2_1/m$ space group with monoclinic crystal structures with a uniform $Nb^{4+}$ chain distance of ∼3.35 Å.[39] For $NbS_3$-II, its complex unit cell structure contains four types of symmetry-related trigonal prismatic (TP) chains, resembling the structure of $NbSe_3$.[40] Polymorph II, in particular, is known to exhibit three CDW phases at $T_{P0}$ ∼ 460 K, $T_{P1}$ ∼ 330−370 K, and $T_{P2}$ ∼ 150 K with considerable change in its resistive profile.[40,43] For this study, we used $NbS_3$ crystals synthesized by the chemical vapor transport (CVT) technique; growth from the elements employed a 973−943 K heating gradient and excess sulfur for transport.[39,44] Figure 1b presents the scanning electron microscopy (SEM) imaging and the corresponding energy-dispersive X-ray spectroscopy (EDS) mapping of the as-grown wire-like $NbS_3$ crystals. It should be noted here that in the present context, the distinction between polymorphs II and V is not that important. Both of the polymorphs are metallic and have CDW phase transitions in the close temperature range. If the mixture of $NbS_3$ fillers used for the ink preparation contains other polymorphs, e.g., $NbS_3$-I, which are semiconducting (and do not have CDW transitions), one can expect that the effects on the resistance of the inks due to the presence of the CDW fillers will be weakened but not suppressed completely.

To verify the electrical characteristics of these $NbS_3$ crystals, we first measured the temperature-dependent electrical resistance of devices fabricated by using *clean* mechanically exfoliated $NbS_3$ nanowires. $NbS_3$ whiskers were mechanically exfoliated into high-aspect-ratio thin nanowire chains on top of a clean $SiO_2$/Si substrate using Nitto tape. To protect the $NbS_3$ nanowire from environmental exposure, a thin *h*-BN layer was transferred on top of the nanowire by using an all-dry transfer method. Contacts were made by patterning the device using e-beam lithography (EBL), followed by etching the *h*-BN protective layer using reactive ion etching (RIE), and finally depositing Ti/Au metals with 10 nm/90 nm thickness in an e-beam evaporation (EBE) chamber. Figure 2a shows an optical microscopy image of a representative *h*-BN-capped $NbS_3$ nanowire device on a $SiO_2$/Si substrate. The electrical properties of the $NbS_3$ device channel were measured in a two-terminal configuration at different temperatures.

The measurements were conducted inside a cryogenic probe station (Lakeshore TTPX) by using a semiconductor parameter analyzer (Agilent B1500A). Figure 2b shows the current−voltage ($I$−$V$) behavior at room temperature. As seen, the $I$−$V$ plot follows a linear ohmic behavior at lower biases with superlinear characteristics after a particular bias point, termed the threshold voltage, $V_{th}$. In the context of CDW phenomena in quasi-1D materials, the linear part of the electric transport behavior is attributed to the current carried by individual electrons. The nonlinearity in $I$−$V$ at and beyond $V_{th}$ is attributed to the collective current produced by the depinning and sliding of the CDW condensate in the incommensurate CDW phase of the material. The total current, $I_{total}$, is a summation of linear current, $I_L$, and collective CDW current, $I_{CDW}$, i.e., $I_{total} = I_L + I_{CDW}$.[45] The temperature-dependent $I$−$V$ plots of the device, shown in Figure 2c, in the temperature range between 150 and 400 K, also followed similar threshold field-dependent $I$−$V$ behavior, indicating the presence of an incommensurate CDW phase across the measured temperature range. More details regarding the depinning of CDW phases in different quasi-1D materials have been reported by some of us and others elsewhere, and it is beyond the scope of this study.[44,46,47]

The resistance, $R$, of the $NbS_3$ nanowire device at different temperatures was extracted from the linear ohmic part of the $I$−$V$ data. The results are presented in Figure 2d (blue symbols) in the semilog scale as a function of the inverse temperature, 1000/$T$. As seen, the resistance increases with an inverse temperature. Two distinguishable sharp changes can be


https://doi.org/10.1021/acsaelm.4c00646
ACS Appl. Electron. Mater. 2024, 6, 4653−4660

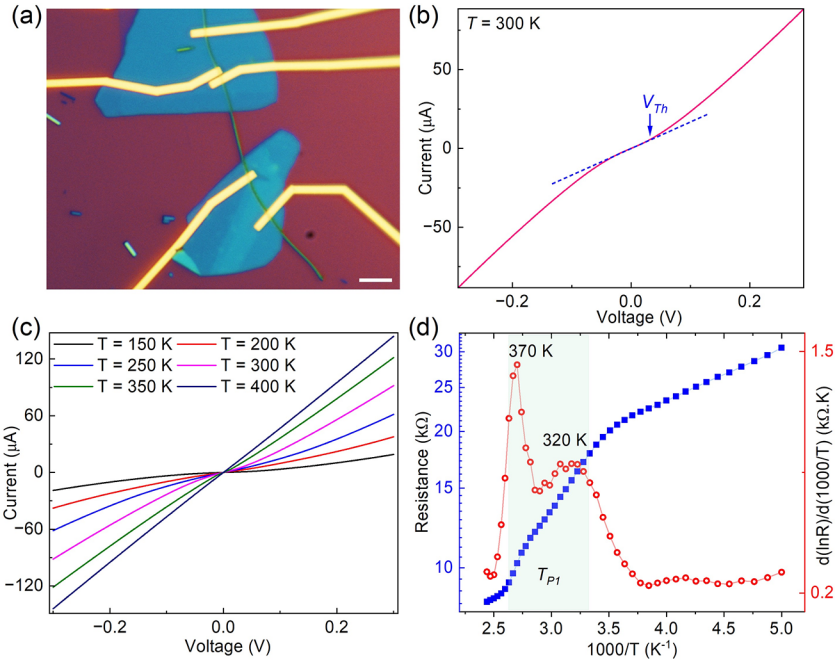


**Figure 2.** (a) Optical microscopy image of a representative $NbS_3$ device. The nanowires were isolated by using mechanical exfoliation and capped with an *h*-BN layer to protect the channel from environmental exposure. The scale bar is 5 $\mu$m. (b) $I-V$ characterization of the $NbS_3$ device at room temperature. The start of nonlinearity, which has been shown with an arrow, is attributed to the depinning and sliding of the CDW quantum condensate and its contribution to total conduction. (c) Temperature-dependent $I-V$ characterization of the $NbS_3$ device in the temperature range of 150−400 K. (d) Electric resistive characteristic of the device plotted as a function of inverse temperature in a semilogarithmic scale, in the temperature range of 150−400 K. The blue and red symbols show the resistance and its temperature derivative, respectively. The derivative data show a sharp peak at 320 K accompanied by a shoulder at 370 K in the vicinity of the CDW phase transition, $T_{P1}$.

detected in the range of ∼320−370 K, around the CDW phase transition temperature, $T_{P1}$. This region is shaded with a green color in the figure for a better visualization. The resistance changes around $T_{P1}$ can be attributed to the CDW Peierls' transition.[40] The derivative of the resistance as a function of temperature, shown by red symbols in Figure 2d, points out more clearly a prominent peak at 370 K accompanied by a smaller shoulder around ∼320 K. This behavior for $NbS_3$ is similar to the transition temperature reported previously for polymorph II and is consistent with a transition to the incommensurate CDW phase in our device.[48,49]

## 3. INK PREPARATION AND PRINTED DEVICE FABRICATION

We now focus on the central aspect of this study, which is the formulation procedure for ink containing $NbS_3$ fillers, tailored for electronic printing applications. We employed an ultrasonication-based liquid-phase exfoliation (LPT) technique to prepare the ink with exfoliated quasi-1D $NbS_3$ fillers. In this technique, a certain amount of the bulk material is added to the proper solvent, and the solution undergoes ultrasonication for a certain period of time. Exfoliation of the bulk material occurs due to microjets and shock waves generated during the collapse of microbubbles induced by liquid cavitation acting on the layered materials.[50,51] Liquid-phase exfoliation is regarded as one of the most cost-effective techniques for the large-scale exfoliation of vdW materials owing to its straightforward mechanics and high adaptability.[52−54]

To break down bulk $NbS_3$ crystals into thinner nanowires, various solvents were tested, including acetone, isopropyl alcohol (IPA), and dimethylformamide (DMF). DMF exhibits the highest efficiency among these solvents, effectively exfoliating more crystals in a relatively short period. Figures 3a and 3b show the optical microscopy and scanning electron microscopy (SEM) images of the CVT-grown bulk $NbS_3$, respectively. Note the needle-like structure of the material, even in the bulk form. To prepare the ink, 5 mg of the bulk $NbS_3$ is added into a 20 mL high-boiling-point DMF solvent (Figure 3c). The mixture underwent exfoliation for 6 h in a low-power bath sonicator (5510 Branson). As seen in Figure 3d, after sonication, the color of the mixture changed from clear to dark brown, confirming an efficient exfoliation and dispersion of bulk $NbS_3$ in DMF. To separate the supernatant and precipitate components, the solution was transferred to a centrifuge tube and underwent centrifugation for 1 h at 2000 rpm. Figure 3e shows the mixture after the centrifugation process. The precipitate component is collected to be used in the final step of the ink preparation, which will be discussed next.

In printing electronics, the thermophysical properties of the ink and the size of the injecting nozzle are key factors in the formation of proper ink droplets with desirable characteristics.[55−59] The droplet formation criteria is determined by the *Z*-number, $Z = \sqrt{\zeta \rho a}/\mu$, a dimensionless parameter in which $\zeta$, $\rho$, and $\mu$ are respectively the surface tension, density, and the dynamic viscosity of the ink solution, and $a$ is the diameter of the injecting nozzle.[60,61] A *Z*-number range of $1 \leq Z \leq 14$ generally results in good droplet formation and its uniform distribution at the intended regions on the substrate.[62] Inks with $Z < 1$ or $Z > 14$ result in elongated ligaments or satellite droplet formation which would result in undesirable printing patterns.[60,63−66] To tune the properties of our ink, we collected the precipitate part of the liquid-phase exfoliated $NbS_3$ and transferred it to a secondary solvent of 5 mL of isopropyl


https://doi.org/10.1021/acsaelm.4c00646
ACS Appl. Electron. Mater. 2024, 6, 4653−4660

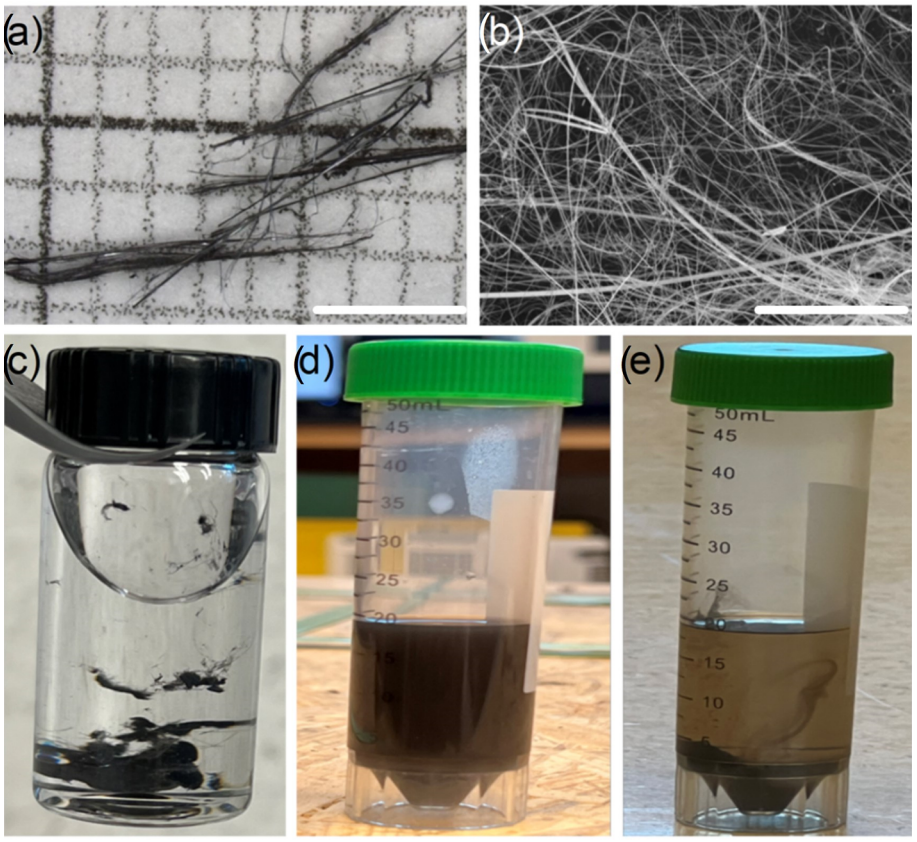


**Figure 3.** (a) Optical microscopy and (b) SEM images of the bulk CVT-grown $NbS_3$ material. Note the quasi-1D needle-like structures of $NbS_3$ even in the bulk form. The scale bars in the optical and SEM images are 2.5 mm and 50 $\mu$m, respectively. (c) Mixture of $NbS_3$ and DMF as solvent before sonication. (d) Solution of $NbS_3$ in DMF after undergoing bath sonication. Note the change in the color of DMF solvent from colorless to dark brown, confirming an efficient exfoliation of $NbS_3$. (e) The same mixture after the centrifugation process. The precipitate part of the mixture, settled at the bottom of the vial, is used for final ink preparation.

alcohol (IPA). The solution underwent a 10 min bath sonication for uniform filler dispersion and to prevent filler agglomeration. Despite the advantageous properties of IPA such as low boiling point and high evaporation rate, IPA-based solutions tend to have high surface tension and low viscosity, resulting in the creation of undesirable "coffee rings" after the drying of the ink on the substrate.[15] To resolve these issues, an equal volume of ethylene glycol (EG) was added to the IPA solution containing $NbS_3$ fillers. EG has a higher boiling, and its addition to the IPA-based solution increases the solvent's boiling point.[63,64] The mixing of two solvents with different boiling points and surface tensions prevents the formation of coffee rings which can be explained by the Marangoni effect.[67,68] Figure 4a shows the resultant ink for printing. The produced $NbS_3$ inks were relatively stable in the air. They demonstrated reproducible results along several thermal cycle measurements within a week. The inks were stored under an inert atmosphere between the measurements for long-term use.

Figure 4b illustrates a schematic representation of the two-terminal printed device used in this study. Prior to the printing, electrodes were made by applying silver (Ag) paste on a Si/$SiO_2$ substrate with a printed channel length of ~1.6 mm. The electrodes were annealed for 40 min at 70 °C using a hot plate. A piezo-driven inkjet printer (Hyrel 30M 3D) with a nozzle diameter of $a$ = 0.21 mm was used to print the ink solution containing $NbS_3$ fillers as the conductive channel between the electrodes. The bed temperature of the printer was kept at 70 °C to expedite the solvent evaporation and ink-drying process and also to mitigate the coffee-ring effect by enhancing the movement of fillers within the ink droplet after deposition. Figure 4c presents a long-shot SEM image of the ink channel. As seen, no coffee rings were observed in the channel, confirming the high quality of the printed device. Figure 4d displays a magnified image of the channel. A network of quasi-1D $NbS_3$ fillers with different aspect ratios, deposited uniformly in the channel, can be seen in this image. Note that some fillers appear as rigid nanoribbons, enclosed by blue dashed lines, while the majority of the fillers have flexible quasi-1D nanowire structures (shown in yellow color). The rigid, needle-like wires most likely are of type I or type IV polymorphs, whereas the fine, hair-type wires more closely resemble type II.[38,44] Given that the ink channel consists of mostly flexible type II $NbS_3$ fillers, one should expect to see signatures of a CDW transition in the printed device similar to the data presented in Figure 2d.

## 4. RESULTS AND DISCUSSION

To examine whether the $NbS_3$-based ink has preserved the CDW properties, we measured the electrical resistance of the printed device in the temperature range of 295−393 K in the heating cycle. We employed the standard two-probe electrical resistance measurements using a multimeter (Fluke 289). The device was heated using a hot plate (Corning PC-4000). A thermocouple was attached to the substrate close to the printed channel to read the temperature of the device at each measurement. Figure 5a presents the resistance of the $NbS_3$ ink


https://doi.org/10.1021/acsaelm.4c00646
ACS Appl. Electron. Mater. 2024, 6, 4653−4660

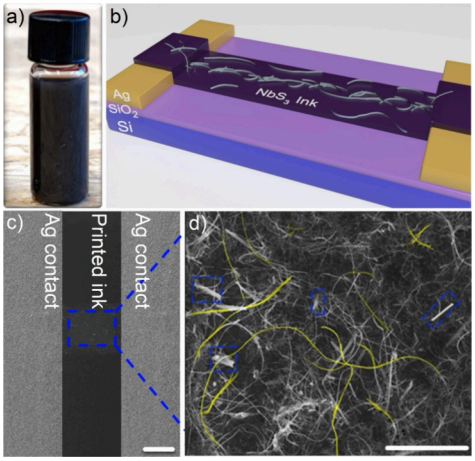


**Figure 4.** (a) $NbS_3$ ink with ethylene glycol and IPA as solvents with mixing volume ratios of 1:1. (b) Schematic showing the basic structure of the printed $NbS_3$ device. (c) SEM image of the printed device showing the $NbS_3$ ink channel and silver paste (Ag) as electrodes. (d) High-resolution zoomed-in SEM image of the printed $NbS_3$ printed ink. The close-up view of the printed $NbS_3$ material exhibits finer details of the ink structure. The "quantum ink" consists of quasi-1D $NbS_3$ fillers of different polymorphs of "rigid needle-like" $NbS_3$-I or $NbS_3$-IV and "flexible hair-like" $NbS_3$-II, with the latter being the predominant phase. Likely $NbS_3$-I and $NbS_3$-II fillers are identified in blue and yellow colors. The dashed blue box in (c) is not to scale with the magnification of the image shown in (d). Scale bars in parts c and d are 20 $\mu$m and 200 nm, respectively.

channel device, $R$, as a function of inverse temperature, 1000/$T$, in a semilog scale. The channel resistance was measured to be ~2 MΩ at RT. As depicted in Figure 5a, the resistance of the channel increases with the temperature increase, with two noticeable variations in the slope occurring at $T \sim 325$ and 375 K. These temperatures correspond to the maxima of the d$R$/d$T$ data shown in Figure 2d and agree well with the CDW transition temperatures reported for single-crystal $NbS_3$-II. These results suggest that $NbS_3$-II preserves its CDW properties despite undergoing liquid-phase exfoliation and printing processes. One should note that defects and disorder are detrimental to any coherent quantum state. While the terminology of what constitutes "quantum" in the CDW context may vary,[69] one can call the CDW phases a macroscopic quantum state given the coherency required for the formation of the condensate and collective transport phenomena. These considerations explain the significance of preserving the CDW phases in the prepared "quantum ink".

To verify that the features observed in the electrical resistance of the prepared inks are associated with the intrinsic properties of $NbS_3$, we prepared a reference graphene-based ink following the same recipe that we used to prepare the $NbS_3$-based ink. Graphene, produced by any methods, does not reveal phase transitions in the examined temperature range. Graphene ink is solely used in this study for comparison with the inks that contain the CDW fillers. Two-terminal devices of a similar design with the same channel length and contacts were printed with graphene ink, and their temperature-dependent electrical resistance was measured. The results of the measurements for $NbS_3$ and graphene ink are presented in Figure 5b. As seen, the electrical resistance of the graphene ink gradually and weakly decreases with heating, showing no detectable anomalies in the slope of its resistance at any examined temperatures. As expected, the resistance of the

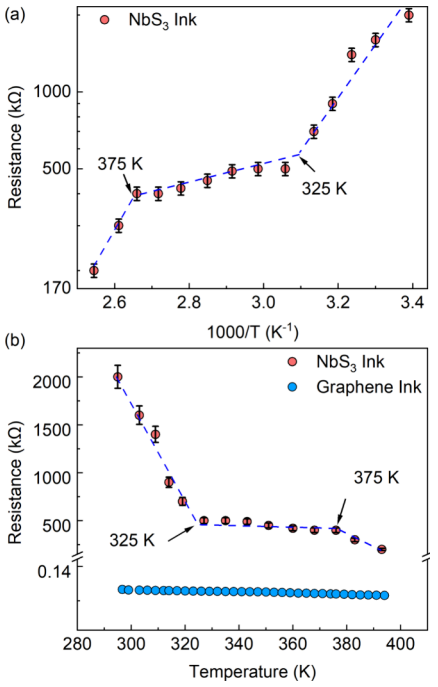


**Figure 5.** (a) Resistance, $R$, of the printed device with the $NbS_3$ ink. The data are plotted as a function of inverse temperature, 1000/$T$, in the semilog scale. Note the onset of the transitions at $T \sim 325$ K and $T \sim 375$ K. (b) $R$ vs $T$ behavior of the reference graphene ink device for comparison with the $NbS_3$ ink device. The temperature-dependent resistance of the graphene ink shows a gradual monotonic drop with temperature rise without any noticeable deviations. In contrast, the $NbS_3$ ink exhibits an obvious change in resistive characteristics at $T \sim 325$ K and $T \sim 375$ K. This comparative approach confirms that the changes in resistive behavior of the ink stem from the CDW phase transition of $NbS_3$-II fillers present within the ink.

channel printed with graphene ink is much lower than that of the channel printed with $NbS_3$ ink. In contrast to the channel printed with graphene ink, the $NbS_3$ ink channel exhibits an obvious change in resistive characteristics at $T \sim 325$ K and $T \sim 375$ K. Based on the comparison with the properties of individual $NbS_3$ fillers (see Figure 2d) and with the properties of the reference ink (Figure 5b), it can be inferred that the nontrivial resistance anomalies observed at these temperatures stem from the CDW phase transitions of $NbS_3$ fillers present within the ink. It is interesting to note that although the $NbS_3$ ink used in this study consists of fillers of different polymorphs, the CDW characteristics can still be observed in the printed device. This finding offers an exciting opportunity for the development of technologically viable and economically feasible CDW-based printed devices.

The temperature-dependent resistive behavior of printed devices can be explained as an interplay between the CDW phase transition of the intrinsic material and the complex transport mechanism of the disordered $NbS_3$ ink channel. Prior studies and the resistive behavior of the device with single-crystal $NbS_3$-II as an active channel, presented in Figure 2d, have shown that $NbS_3$ crystals undergo CDW phase transitions within a wide temperature span, encompassing the range of 325−370 K. In the ink device, a sharp change in resistance is also observed in a similar temperature interval, between $T$ = 314 and 376 K. However, unlike the device with single-crystal $NbS_3$-II, the resistance change is not continuous but slows down at intermediate temperatures. The overall carrier


https://doi.org/10.1021/acsaelm.4c00646
ACS Appl. Electron. Mater. 2024, 6, 4653−4660

conduction process in disordered systems such as inks is governed by hopping charge transport between the delocalized sites of the adjacent fillers.[15,70] The hopping transport behavior typically reveals itself via low values of the electron mobility and specific temperature dependence, i.e., increasing mobility with increasing temperature. However, in inks with CDW fillers, the transport is also affected by the CDW transitions of individual $NbS_3$ fillers in the percolated network of fillers. Other factors such as random interconnections and interfaces between $NbS_3$ fillers, defects, and impurities introduced during the LPE process and the subsequent printing steps also influence the transport properties.[71,72] As a result, charge carrier transport through random networks can be significantly different from that in single-crystal materials. This explains the slower resistance change in the intermediate temperatures, which deviates from the continued sharp resistive change observed in single-crystal $NbS_3$-II at temperatures across the CDW phase transition.

## 5. CONCLUSIONS

In summary, we presented the development of functional "quantum inks" containing quasi-1D $NbS_3$ CDW fillers tailored for inkjet printing applications. The ink formulation involved liquid-phase exfoliation of bulk $NbS_3$ in DMF, followed by dispersing high-aspect-ratio $NbS_3$ fillers in a mixture of ethylene glycol and IPA. Two-terminal devices were printed using the formulated $NbS_3$ ink, and graphene ink as a reference, on $Si/SiO_2$ substrates. Electrical resistance measurements of $NbS_3$ devices exhibited notable changes at $T \sim 330$ K and $T \sim 370$ K. Such changes in resistive behavior were not observed for the reference printed devices with graphene ink. The observed anomalies are attributed to the CDW transitions of individual $NbS_3$ fillers of type II present in the ink. Our findings validate that $NbS_3$-II maintains its intrinsic CDW properties despite undergoing rigorous chemical exfoliation processes. These outcomes are significant for advancing functional inks utilizing quasi-1D fillers with CDW properties, promising a wide array of applications in printed electronics.

## ■ ASSOCIATED CONTENT

### Data Availability Statement

The data that support the findings of this study are available from the corresponding author upon reasonable request.

## ■ AUTHOR INFORMATION


### Corresponding Authors

**Fariborz Kargar** − *Materials Research and Education Center, Department of Mechanical Engineering, Auburn University, Auburn, Alabama 36849, United States;* orcid.org/0000-0003-2192-2023; Email: fkargar@auburn.edu

**Alexander A. Balandin** − *Department of Materials Science and Engineering, University of California, Los Angeles, Los Angeles, California 90095, United States; California NanoSystems Institute, University of California, Los Angeles, Los Angeles, California 90095, United States;* orcid.org/0000-0002-9944-7894; Email: balandin@seas.ucla.edu

### Authors

**Tekwam Geremew** − *Department of Materials Science and Engineering, University of California, Los Angeles, Los Angeles, California 90095, United States; California NanoSystems Institute, University of California, Los Angeles, Los Angeles, California 90095, United States*

**Maedeh Taheri** − *Department of Materials Science and Engineering, University of California, Los Angeles, Los Angeles, California 90095, United States; California NanoSystems Institute, University of California, Los Angeles, Los Angeles, California 90095, United States*

**Nicholas Sesing** − *Department of Chemistry, University of Georgia, Athens, Georgia 30602, United States;* orcid.org/0000-0003-2162-0236

**Subhajit Ghosh** − *Department of Materials Science and Engineering, University of California, Los Angeles, Los Angeles, California 90095, United States; California NanoSystems Institute, University of California, Los Angeles, Los Angeles, California 90095, United States;* orcid.org/0000-0002-7350-5953

**Tina T. Salguero** − *Department of Chemistry, University of Georgia, Athens, Georgia 30602, United States;* orcid.org/0000-0001-9396-3583

Complete contact information is available at: https://pubs.acs.org/10.1021/acsaelm.4c00646


### Author Contributions

A.A.B. and F.K. conceived the idea, coordinated the project, contributed to experimental data analysis, and led the manuscript preparations. T.G. developed the ink, printed devices, measured the electrical properties, and contributed to the data analyses; M.T. fabricated nanodevices, conducted SEM characterization, $I-V$ measurements, and contributed to data analyses; N.S. synthesized bulk crystals by CVT; S.G. contributed to the experimental data analyses; T.T.S. supervised the material growth and contributed to data analysis. All authors participated in the manuscript preparation.

### Notes

The authors declare no competing financial interest.

## ■ ACKNOWLEDGMENTS

The work at UCLA was supported, in part, via the Vannevar Bush Faculty Fellowship (VBFF) to A.A.B. under the Office of Naval Research (ONR) contract N00014-21-1-2947 on One-Dimensional Quantum Materials. A.A.B. also acknowledges the support from the National Science Foundation (NSF) program Designing Materials to Revolutionize and Engineer our Future (DMREF) via a project DMR-1921958 entitled Collaborative Research: Data-Driven Discovery of Synthesis Pathways and Distinguishing Electronic Phenomena of 1D van der Waals Bonded Solids.

## ■ REFERENCES

(1) Yan, K.; Li, J.; Pan, L.; Shi, Y. Inkjet Printing for Flexible and Wearable Electronics. *APL Materials* **2020**, *8* (12), 120705.

(2) Song, O.; Rhee, D.; Kim, J.; Jeon, Y.; Mazánek, V.; Söll, A.; Kwon, Y. A.; Cho, J. H.; Kim, Y. H.; Sofer, Z.; Kang, J. All Inkjet-Printed Electronics Based on Electrochemically Exfoliated Two-Dimensional Metal, Semiconductor, and Dielectric. *npj 2D Mater. Appl.* **2022**, *6* (1), 1−12.

(3) Das, C. M.; Kang, L.; Ouyang, Q.; Yong, K. T. Advanced Low-Dimensional Carbon Materials for Flexible Devices. *InfoMat* **2020**, *2* (4), 698−714.

(4) Kell, A. J.; Paquet, C.; Mozenson, O.; Djavani-Tabrizi, I.; Deore, B.; Liu, X.; Lopinski, G. P.; James, R.; Hettak, K.; Shaker, J.; Momciu, A.; Ferrigno, J.; Ferrand, O.; Hu, J. X.; Lafrenière, S.; Malenfant, P. R. L. Versatile Molecular Silver Ink Platform for Printed Flexible Electronics. *ACS Appl. Mater. Interfaces* **2017**, *9* (20), 17226−17237.

(5) Wu, Z.; Liu, S.; Hao, Z.; Liu, X. MXene Contact Engineering for Printed Electronics. *Advanced Science* **2023**, 1−41.

(6) Kumar, S.; Bhushan, P.; Pandey, M.; Bhattacharya, S. Additive Manufacturing as an Emerging Technology for Fabrication of Microelectromechanical Systems (MEMS). *Journal of Micromanufacturing* **2019**, *2* (2), 175−197.
(7) Zolfaghari, A.; Chen, T.; Yi, A. Y. Additive Manufacturing of Precision Optics at Micro and Nanoscale. *International Journal of Extreme Manufacturing* **2019**, *1* (1), 012005.
(8) Nair, N. M.; Pakkathillam, J. K.; Kumar, K.; Arunachalam, K.; Ray, D.; Swaminathan, P. Printable Silver Nanowire and PEDOT:PSS Nanocomposite Ink for Flexible Transparent Conducting Applications. *ACS Appl. Electron. Mater.* **2020**, *2* (4), 1000−1010.
(9) Sajedi-Moghaddam, A.; Rahmanian, E.; Naseri, N. Inkjet-Printing Technology for Supercapacitor Application: Current State and Perspectives. *ACS Appl. Mater. Interfaces* **2020**, *12* (31), 34487−34504.
(10) Hussain, A.; Abbas, N.; Ali, A. Inkjet Printing: A Viable Technology for Biosensor Fabrication. *Chemosensors* **2022**, *10* (3), 103.
(11) Karunakaran, S. K.; Arumugam, G. M.; Yang, W.; Ge, S.; Khan, S. N.; Lin, X.; Yang, G. Recent Progress in Inkjet-Printed Solar Cells. *J. Mater. Chem. A* **2019**, *7* (23), 13873−13902.
(12) Mattana, G.; Loi, A.; Woytasik, M.; Barbaro, M.; Noël, V.; Piro, B. Inkjet-Printing: A New Fabrication Technology for Organic Transistors. *Advanced Materials Technologies* **2017**, *2* (10), 1−27.
(13) Castrejon-Pita, J. R.; Baxter, W. R. S.; Morgan, J.; Temple, S.; Martin, G. D.; Hutchings, I. M. Future, Opportunities and Challenges of Inkjet Technologies. *Atomization and Sprays* **2013**, *23* (6), 541−565.
(14) Li, D.; Lai, W. Y.; Zhang, Y. Z.; Huang, W. Printable Transparent Conductive Films for Flexible Electronics. *Adv. Mater.* **2018**, *30* (10), 1−24.
(15) Baraghani, S.; Abourahma, J.; Barani, Z.; Mohammadzadeh, A.; Sudhindra, S.; Lipatov, A.; Sinitskii, A.; Kargar, F.; Balandin, A. A. Printed Electronic Devices with Inks of $TiS_3$ Quasi-One-Dimensional van Der Waals Material. *ACS Appl. Mater. Interfaces* **2021**, *13* (39), 47033−47042.
(16) Li, C.; Bu, F.; Wang, Q.; Liu, X. Recent Developments of Inkjet-Printed Flexible Energy Storage Devices. *Advanced Materials Interfaces* **2022**, *9* (34), 1−20.
(17) Arrabito, G.; Aleeva, Y.; Pezzilli, R.; Ferrara, V.; Medaglia, P. G.; Pignataro, B.; Prestopino, G. Printing Zno Inks: From Principles to Devices. *Crystals* **2020**, *10* (6), 449.
(18) Zhang, Y.; Shi, G.; Qin, J.; Lowe, S. E.; Zhang, S.; Zhao, H.; Zhong, Y. L. Recent Progress of Direct Ink Writing of Electronic Components for Advanced Wearable Devices. *ACS Appl. Electron. Mater.* **2019**, *1* (9), 1718−1734.
(19) Tran, T. S.; Dutta, N. K.; Choudhury, N. R. Graphene Inks for Printed Flexible Electronics: Graphene Dispersions, Ink Formulations, Printing Techniques and Applications. *Adv. Colloid Interface Sci.* **2018**, *261*, 41−61.
(20) Kralj, M.; Krivačić, S.; Ivanišević, I.; Zubak, M.; Supina, A.; Marciuš, M.; Halasz, I.; Kassal, P. Conductive Inks Based on Melamine Intercalated Graphene Nanosheets for Inkjet Printed Flexible Electronics. *Nanomaterials* **2022**, *12* (17), 2936.
(21) Barmpakos, D.; Belessi, V.; Xanthopoulos, N.; Krontiras, C. A.; Kaltsas, G. Flexible Inkjet-Printed Heaters Utilizing Graphene-Based Inks. *Sensors* **2022**, *22* (3), 1−10.
(22) Ng, L. W. T.; Howe, R. C. T.; Yang, Z.; Hasan, T.; Hu, G.; Zhu, X.; Jones, C. G. *Printing of Graphene and Related 2D Materials: Technology, Formulation and Applications*; Springer: 2018.
(23) Conti, S.; Calabrese, G.; Parvez, K.; Pimpolari, L.; Pieri, F.; Iannaccone, G.; Casiraghi, C.; Fiori, G. Printed Transistors Made of 2D Material-Based Inks. *Nat. Rev. Mater.* **2023**, *8* (10), 651−667.
(24) Pinilla, S.; Coelho, J.; Li, K.; Liu, J.; Nicolosi, V. Two-Dimensional Material Inks. *Nat. Rev. Mater.* **2022**, *7* (9), 717−735.
(25) Cho, K.; Lee, T.; Chung, S. Inkjet Printing of Two-Dimensional van Der Waals Materials: A New Route towards Emerging Electronic Device Applications. *Nanoscale Horizons* **2022**, *7* (10), 1161−1176.
(26) Peng, M.; Wen, Z.; Sun, X. Recent Progress of Flexible Photodetectors Based on Low-Dimensional II-VI Semiconductors and Their Application in Wearable Electronics. *Adv. Funct. Mater.* **2023**, *33* (11), 1−24.
(27) Ippolito, S.; Urban, F.; Zheng, W.; Mazzarisi, O.; Valentini, C.; Kelly, A. G.; Gali, S. M.; Bonn, M.; Beljonne, D.; Corberi, F.; Coleman, J. N.; Wang, H. I.; Samorì, P. Unveiling Charge-Transport Mechanisms in Electronic Devices Based on Defect-Engineered $MoS_2$ Covalent Networks. *Adv. Mater.* **2023**, *35* (15), 2211157.
(28) Park, S.; Kim, H.; Kim, J.-H.; Yeo, W.-H. Advanced Nanomaterials, Printing Processes, and Applications for Flexible Hybrid Electronics. *Materials* **2020**, *13*, 3587.
(29) Verboven, I.; Deferme, W. Printing of Flexible Light Emitting Devices: A Review on Different Technologies and Devices, Printing Technologies and State-of-the-Art Applications and Future Prospects. *Prog. Mater. Sci.* **2021**, *118*, 100760.
(30) Xi, X.; Zhao, L.; Wang, Z.; Berger, H.; Forró, L.; Shan, J.; Mak, K. F. Strongly Enhanced Charge-Density-Wave Order in Monolayer $NbSe_2$. *Nat. Nanotechnol.* **2015**, *10* (9), 765−769.
(31) Grüner, G. The Dynamics of Charge-Density Waves. *Reviews of modern physics* **1988**, *60* (4), 1129.
(32) Ghosh, S.; Kargar, F.; Sesing, N. R.; Barani, Z.; Salguero, T. T.; Yan, D.; Rumyantsev, S.; Balandin, A. A. Low-Frequency Current Fluctuations in Quasi-1D $(TaSe_4)_2I$ Weyl Semimetal Nanoribbons. *Adv. Electron. Mater.* **2023**, *9* (2), 2200860.
(33) Balandin, A. A.; Zaitsev-Zotov, S. V.; Grüner, G. Charge-Density-Wave Quantum Materials and Devices - New Developments and Future Prospects. *Appl. Phys. Lett.* **2021**, *119* (17), 9−11.
(34) Zhu, C.; Chen, Y.; Liu, F.; Zheng, S.; Li, X.; Chaturvedi, A.; Zhou, J.; Fu, Q.; He, Y.; Zeng, Q.; Fan, H. J.; Zhang, H.; Liu, W. J.; Yu, T.; Liu, Z. Light-Tunable 1T-$TaS_2$ Charge-Density-Wave Oscillators. *ACS Nano* **2018**, *12* (11), 11203−11210.
(35) Liu, G.; Debnath, B.; Pope, T. R.; Salguero, T. T.; Lake, R. K.; Balandin, A. A. A Charge-Density-Wave Oscillator Based on an Integrated Tantalum Disulfide-Boron Nitride-Graphene Device Operating at Room Temperature. *Nat. Nanotechnol.* **2016**, *11* (10), 845−850.
(36) Conejeros, S.; Guster, B.; Alemany, P.; Pouget, J.-P.; Canadell, E. Rich Polymorphism of Layered $NbS_3$. *Chem. Mater.* **2021**, *33*, 5449−5463.
(37) Chen, M.; Li, L.; Xu, M.; Li, W.; Zheng, L.; Wang, X. Quasi-One-Dimensional van Der Waals Transition Metal Trichalcogenides. *Research* **2023**, *6*, 0066.
(38) Bloodgood, M. A.; Ghafouri, Y.; Wei, P.; Salguero, T. T. Impact of the Chemical Vapor Transport Agent on Polymorphism in the Quasi-1D $NbS_3$ system. *Appl. Phys. Lett.* **2022**, *120* (17), 173103.
(39) Bloodgood, M. A.; Wei, P.; Aytan, E.; Bozhilov, K. N.; Balandin, A. A.; Salguero, T. T. Monoclinic Structures of Niobium Trisulfide. *APL Materials* **2018**, *6* (2), 026602.
(40) Zybtsev, S. G.; Pokrovski, V. Y.; Nasretdinova, V. F.; Zaitsev-Zotov, S. V.; Pavlovskiy, V. V.; Odobesco, A. B.; Pai, W. W.; Chu, M.-W. W.; Lin, Y. G.; Zupanič, E.; Van Midden, H. J. P.; Šturm, S.; Tchernychova, E.; Prodan, A.; Bennett, J. C.; Mukhamedshin, I. R.; Chernysheva, O. V.; Menushenkov, A. P.; Loginov, V. B.; Loginov, B. A.; Titov, A. N.; Abdel-Hafiez, M. $NbS_3$: A Unique Quasi-One-Dimensional Conductor with Three Charge Density Wave Transitions. *Phys. Rev. B* **2017**, *99* (3), 39901.
(41) Barani, Z.; Kargar, F.; Ghafouri, Y.; Ghosh, S.; Godziszewski, K.; Baraghani, S.; Yashchyshyn, Y.; Cywiński, G.; Rumyantsev, S.; Salguero, T. T.; Balandin, A. A. Electrically Insulating Flexible Films with Quasi-1D van Der Waals Fillers as Efficient Electromagnetic Shields in the GHz and Sub-THz Frequency Bands. *Adv. Mater.* **2021**, *33* (11), 1−9.
(42) Zupanič, E.; Van Midden, H. J. P.; Van Midden, M. A.; Šturm, S.; Tchernychova, E.; Pokrovskii, V. Y.; Zybtsev, S. G.; Nasretdinova, V. F.; Zaitsev-Zotov, S. V.; Chen, W. T.; Pai, W. W.; Bennett, J. C.; Prodan, A. Basic and Charge Density Wave Modulated Structures of NbS3-II. *Phys. Rev. B* **2018**, *98* (17), 1−12.


https://doi.org/10.1021/acsaelm.4c00646
ACS Appl. Electron. Mater. 2024, 6, 4653−4660

(43) Eni. Charge-Density-Wave Transport above Room Temperature in Polytype of $NbS_3$. *Angewandte Chemie International Edition, 6(11), 951−952.* **1967**, *40* (Mi), 5−24.
(44) Taheri, M.; Sesing, N.; Salguero, T. T.; Balandin, A. A. Electric-Field Modulation of the Charge-Density-Wave Quantum Condensate in h-BN/$NbS_3$ Quasi-2D/1D Heterostructure Devices. *Appl. Phys. Lett.* **2023**, *123* (23), 233101.
(45) Ido, M.; Kawabata, K.; Sambongi, T.; Yamaya, K.; Abe, Y. Nonlinear Transport Phenomena in $MX_3$. *Mol. Cryst. Liq. Cryst.* **1982**, *81*, 91−97.
(46) Fleming, R. M. Electric-Field Depinning of Charge-Density Waves in $NbSe_3$. *Phys. Rev. B* **1980**, *22* (12), 5606−5612.
(47) Grüner, G.; Zawadowski, A.; Chaikin, P. M. Nonlinear Conductivity and Noise Due to Charge-Density-Wave Depinning in $NbSe_3$. *Phys. Rev. Lett.* **1981**, *46* (7), 511−515.
(48) Zybtsev, S.; Pokrovskii, V.; Nasretdinova, V.; Zaitsev-Zotov, S.; Zupanič, E.; van Midden, M.; Pai, L. The Ultra-High-TP Charge-Density Wave in the Monoclinic Phase of $NbS_3$. *J. Alloys Compd.* **2021**, *854*, 157098.
(49) Zybtsev, S. G.; Pokrovskii, V. Y.; Nasretdinova, V. F.; Zaitsev-Zotov, S. V. Gigahertz-Range Synchronization at Room Temperature and Other Features of Charge-Density Wave Transport in the Quasi-One-Dimensional Conductor $NbS_3$. *Appl. Phys. Lett.* **2009**, *94* (15), 152112.
(50) Vidal, J. L.; Gallant, S. M. V.; Connors, E. P.; Richards, D. D.; Macquarrie, S. L.; Kerton, F. M. Green Solvents for the Liquid-Phase Exfoliation of Biochars. *ACS Sustainable Chem. Eng.* **2021**, *9* (27), 9114−9125.
(51) Hu, C. X.; Shin, Y.; Read, O.; Casiraghi, C. Dispersant-Assisted Liquid-Phase Exfoliation of 2D Materials beyond Graphene. *Nanoscale* **2021**, *13* (2), 460−484.
(52) Li, Y.; Kuang, G.; Jiao, Z.; Yao, L.; Duan, R. Recent Progress on the Mechanical Exfoliation of 2D Transition Metal Dichalcogenides. *Materials Research Express* **2022**, *9* (12), 122001.
(53) Li, Z.; Young, R. J.; Backes, C.; Zhao, W.; Zhang, X.; Zhukov, A. A.; Tillotson, E.; Conlan, A. P.; Ding, F.; Haigh, S. J.; Novoselov, K. S.; Coleman, J. N. Mechanisms of Liquid-Phase Exfoliation for the Production of Graphene. *ACS Nano* **2020**, *14* (9), 10976−10985.
(54) Chavalekvirat, P.; Hirunpinyopas, W.; Deshsorn, K.; Jitapunkul, K.; Iamprasertkun, P. Liquid Phase Exfoliation of 2D Materials and Its Electrochemical Applications in the Data-Driven Future. *Precis. Chem.* **2024**.
(55) Bastola, A.; He, Y.; Im, J.; Rivers, G.; Wang, F.; Worsley, R.; Austin, J. S.; Nelson-Dummett, O.; Wildman, R. D.; Hague, R.; Tuck, C. J.; Turyanska, L. Formulation of Functional Materials for Inkjet Printing: A Pathway towards Fully 3D Printed Electronics. *Materials Today Electronics* **2023**, *6*, 100058.
(56) Zhao, D.; Zhou, H.; Wang, Y.; Yin, J.; Huang, Y. Drop-on-Demand (DOD) Inkjet Dynamics of Printing Viscoelastic Conductive Ink. *Additive Manufacturing* **2021**, *48* (PB), 102451.
(57) Han, Y. J.; Kim, D. Y.; An, K.; Kang, K. T.; Ju, B. K.; Cho, K. H. Sequential Improvement from Cosolvents Ink Formulation to Vacuum Annealing for Ink-Jet Printed Quantum-Dot Light-Emitting Diodes. *Materials* **2020**, *13* (21), 1−14.
(58) Zhong, Y.; Fang, H.; Ma, Q.; Dong, X. Analysis of Droplet Stability after Ejection from an Inkjet Nozzle. *J. Fluid Mech.* **2018**, *845* (May), 378−391.
(59) Gao, C.; Zhang, Y.; Mia, S.; Xing, T.; Chen, G. Development of Inkjet Printing Ink Based on Component Solubility Parameters and Its Properties. *Colloids Surf., A* **2021**, *609*, 125676.
(60) Arango, J. C.; Pintro, C. J.; Singh, A.; Claridge, S. A. Inkjet Printing of Nanoscale Functional Patterns on 2D Crystalline Materials and Transfer to Soft Materials. *ACS Appl. Mater. Interfaces* **2024**, *16* (6), 8055−8065.
(61) He, B.; Yang, S.; Qin, Z.; Wen, B.; Zhang, C. The Roles of Wettability and Surface Tension in Droplet Formation during Inkjet Printing. *Sci. Rep.* **2017**, *7* (1), 1−7.
(62) Kim, S.; Cho, M.; Jung, S. The Design of an Inkjet Drive Waveform Using Machine Learning. *Sci. Rep.* **2022**, *12* (1), 1−10.
(63) Jafarpour, M.; Nüesch, F.; Heier, J.; Abdolhosseinzadeh, S. Functional Ink Formulation for Printing and Coating of Graphene and Other 2D Materials: Challenges and Solutions. *Small Science* **2022**, *2* (11), 2200040.
(64) Jun, H. Y.; Kim, S. J.; Choi, C. H. Ink Formulation and Printing Parameters for Inkjet Printing of Two Dimensional Materials: A Mini Review. *Nanomaterials* **2021**, *11* (12), 3441.
(65) Nargatti, K. I.; Pathak, T. S.; Ahankari, S. S.; Dizon, J. R. C.; Subramaniam, R. T. Graphene-Based Inks for Flexible Supercapacitor Electrodes: A Review. *ACS Appl. Electron. Mater.* **2024**, *6* (1), 24−46.
(66) Liu, Y.; Derby, B. Experimental Study of the Parameters for Stable Drop-on-Demand Inkjet Performance. *Phys. Fluids* **2019**, *31* (3), 032004.
(67) Sun, J.; Bao, B.; He, M.; Zhou, H.; Song, Y. Recent Advances in Controlling the Depositing Morphologies of Inkjet Droplets. *ACS Appl. Mater. Interfaces* **2015**, *7* (51), 28086−28099.
(68) Hu, H.; Larson, R. G. Marangoni Effect Reverses Coffee-Ring Depositions. *J. Phys. Chem. B* **2006**, *110* (14), 7090−7094.
(69) Miller, J. H.; Wijesinghe, A. I.; Tang, Z.; Guloy, A. M. Coherent Quantum Transport of Charge Density Waves. *Physical Review B - Condensed Matter and Materials Physics* **2013**, *87* (11), 1−12.
(70) Zhang, L.; Shi, X.-L. L.; Yang, Y.-L. L.; Chen, Z.-G. G. Flexible Thermoelectric Materials and Devices: From Materials to Applications. *Mater. Today* **2021**, *46* (June), 62−108.
(71) Frisenda, R.; Giovanelli, E.; Mishra, P.; Gant, P.; Flores, E.; Sánchez, C.; Ares, J. R.; Perez De Lara, D.; Ferrer, I. J.; Pérez, E. M.; Castellanos-Gomez, A. Dielectrophoretic Assembly of Liquid-Phase-Exfoliated $TiS_3$ Nanoribbons for Photodetecting Applications. *Chem. Commun.* **2017**, *53* (45), 6164−6167.
(72) Vasilijević, S.; Mattana, G.; Anquetin, G.; Battaglini, N.; Piro, B. Electrochemical Tuning of Reduced Graphene Oxide in Printed Electrolyte-Gated Transistors. Impact on Charge Transport Properties. *Electrochim. Acta* **2021**, *371*, 137819.


https://doi.org/10.1021/acsaelm.4c00646
ACS Appl. Electron. Mater. 2024, 6, 4653−4660